Mater. Res. Soc. Symp. Proc. Vol. 1026 © 2008 Materials Research Society 1026-C16-02

# Reduction of Contrast in ADF-STEM Images Due To Amorphous Layer

Sara Maccagnano-Zacher, Andre Mkhoyan, and John Silcox
Applied and Engineering Physics, Cornell University, Ithaca, NY, 14853

## ABSTRACT

A study of high-resolution ADF imaging in aberration-corrected STEMs was carried out by multislice simulation. The presence of amorphous layers at the surface of a crystalline specimen is shown to significantly alter the visibility of the atomic columns in ADF images. After propagating through an amorphous layer a portion of the beam passes without any alteration while scattered electrons introduce a Gaussian background. An amorphous layer at the beam entry surface appears to have slightly more of an effect on the ADF image contrast than that of an amorphous layer at the exit surface, and this difference increases with increasing atomic number. With a constant crystal layer thickness, the reduction of contrast as a function of increasing amorphous layer is found to have the same behavior and trend, regardless of the initial crystal layer thickness.

## INTRODUCTION

Very often layers of amorphous material are present on the surfaces of crystalline specimens prepared for study in conventional transmission electron microscopes (TEMs) or scanning-TEMs (STEMs). The reasons for the presence of the amorphous layers in these specimens vary. Preparation of thin, electron-transparent specimens is often carried out by manual polishing [1–3] or ion milling [4,5]. Both methods almost always result in the creation of amorphous layers on the polished/milled surfaces, although the thickness of these layers varies with technique, setup and operator skills. Amorphous carbon films often serve as supports for specimens such as quantum dots, rods and wires. In some cases specimens are sensitive to electron-beam-induced knock-on damage [7,6]. For these samples the surfaces can be intentionally covered with a layer of amorphous carbon for protection [7]. Electron-beam-induced damage itself creates pockets of amorphous material, at locations in the crystal that are uncertain but with effects that will be consequential in the resulting ADF image.

The presence of an amorphous layer on the surfaces of crystalline specimens is expected to have an effect on high-resolution annular dark field (ADF) imaging, and multislice simulations in a previous study [8] have found amorphous material to cause a marked reduction in contrast. This paper explores the effect varying thicknesses of amorphous material have on the contrast of ADF STEM images.

## MULTISLICE ADF-STEM SIMULATIONS

The algorithm for calculation of the ADF-STEM images is based on the multislice method [9], and a more detailed discussion of the method as used in these simulations is given in [8]. The ADF-STEM simulations presented in this paper were performed primarily on silicon specimens in the [110] crystal orientation with added layers of silicon amorphous material. The sizes of the Si supercells used in the calculations were: 27.15×26.88 Å. The images were obtained by scanning the probe over a 12×12 Å area in the middle of the supercell with 70×70 steps, and the contrast of these images was subsequently obtained. The slice thickness used for Si crystals aligned along the [110] was 1.920 Å, and the inner and outer angles of the ADF detector were 54 and 240 mrads. All calculated ADF intensities are normalized with respect to the incident beam and, because the incident probe intensities in all calculations are kept the same, they are all normalized to the same value. This normalization to a single incident electron is essential for a quantitative comparison of different ADF intensities.

Contrast values for each ADF image is obtained by taking the average intensity value from the atomic column locations, $I_{max}$, the areas between the atomic columns, $I_{min}$, and the average intensity value of the entire image, $I_{mean}$. The value for the contrast is found by subtracting $I_{min}$ from $I_{max}$ and dividing by $I_{mean}$. This formula was chosen so that images with high definition of atomic columns have a large contrast value, whereas images of amorphous materials have a contrast value of zero.

The STEM probe used for the simulations in this paper is one whose axial aberrations have been corrected, creating a spatially focused probe of ~0.8 Å, close to the conditions used in [10]: acceleration voltage of 100 kV, $C_{s(3)}$=- 0.015 mm, $C_5$=10 mm, objective angle of 25 mrad, and defocus of -30 Å. A plot of the intensity of this probe is shown in Figure 1.

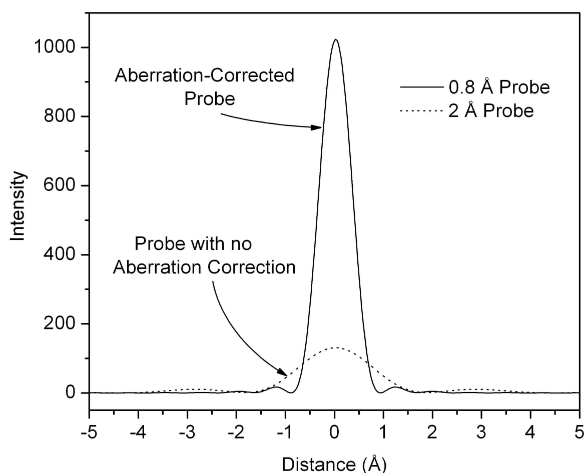


**Figure 1:** The intensity of the STEM probe used in the multislice simulations in this study (solid line). The plot of a probe with no axial corrections is also shown for comparison (dashed line).

## RESULTS AND DISCUSSION

The contrast of ADF STEM images was calculated for Si samples in the [110] orientation for samples that were half amorphous and half crystal. The thickness of the total sample was varied, and the contrast for each thickness is plotted in Figure 2(A).

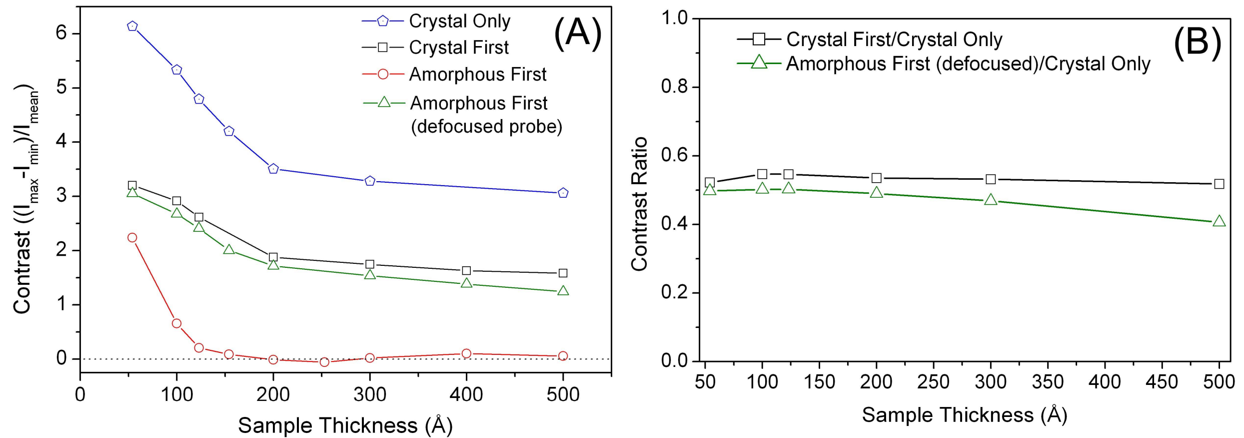


**Figure 2:** The ADF image contrast for varying sample thickness is shown, where each sample (except "crystal only") is constructed of 50% crystal and 50% amorphous material. In (A), the top data shows the contrast of the crystal layer only, whose thickness is half the corresponding value on the x-axis. The other data plots show the reduction in contrast with the addition of an amorphous layer with the same thickness as the crystal layer, where the total sample is oriented with the crystal at the entry surface (open square), the amorphous at the entry surface and the probe defocused to focus on the crystal (open triangle), and the amorphous at the entry surface with the probe focused on top surface (open circle). (B) shows the ratio of the contrast values of the middle two data plots in (A) with the crystal only contrast.

First, to obtain a baseline contrast with which to compare other contrast values, just the crystal layer with no amorphous material was simulated. The thickness of the crystal for this simulation was half the value of the total sample thickness of all crystal/amorphous simulations, and therefore half the thickness of the x-axis value in Figure 2(A). To observe contrast reduction due to amorphous layers, an amorphous layer was added to the crystal layer. The sample was placed so that the crystal was at the entry surface and the probe focused on the entry surface. It was also oriented such that the amorphous layer was placed at the entry surface with the probe focused in two ways: the probe focused on the top surface, and with the probe focused on the crystal layer that begins at the center of the sample (termed 'defocused probe'). In the first case, with the crystal layer first, a large contrast reduction is seen of about 50% of the crystal only contrast. In the case with the amorphous first and a 'defocused probe', the contrast is slightly below that value, but showing the same behavior and trends. The contrast from a sample with the amorphous layer first and the probe focused on the top of the amorphous layer is very low, quickly reducing to zero. This is what is expected, since the amorphous layer acts only to defocus the probe and scatter it somewhat, so that by the time the probe reaches the crystal layer it is too defocused to resolve any crystal structure. This result was just as was seen in the previous study [8]. The plot in Figure 2B shows the ratio of the image contrasts of the crystal first and amorphous first (with the probe focused at the center of the sample) results and the

crystal only result.  Even though the thickness of the crystal layer is changing, the amorphous layer in both cases serve to reduce the contrast by about half, with the crystal layer first case showing slightly less contrast reduction.  The gap of contrast between these two cases is interesting, due most likely to the scattering influence of the amorphous layer.  When the amorphous layer comes first, it will scatter the probe causing a Gaussian-like background to be created as well as a probe that is simply defocused.  This background scatter is enough to create less contrast in the subsequent image of the crystal sample.  The Gaussian-like background is increased for amorphous samples of greater Z-values [8], so it should be expected that the gap in contrast between crystal first and amorphous first (‘defocused probe’) would be greater for samples with larger Z.  The plot showing these contrast values is shown in Figure 3.

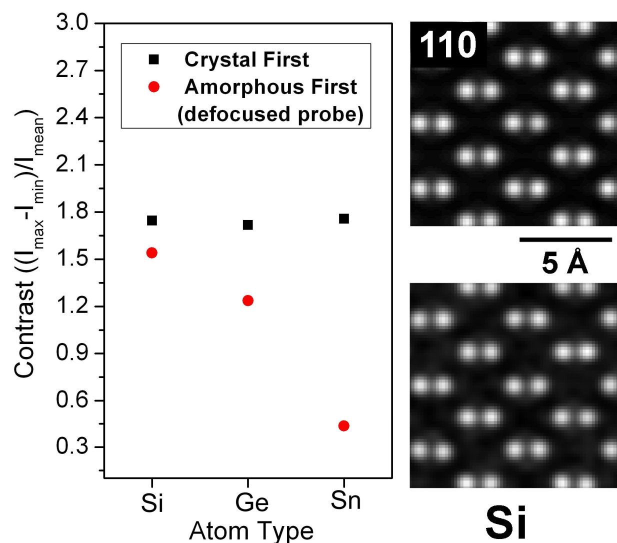


**Figure 3:** (Left) The ADF image contrast values for three different hypothetical materials: Si, Ge and Sn. The crystal structure and lattice constants were those used for Si [110], with only the atomic type changed for each input file. The thickness of each sample is 300Å, with half the sample crystal and half amorphous material. (Right) Simulated ADF images of the Si samples from which contrast values were obtained and presented on the left panel: crystal first (top panel) and amorphous first (bottom panel).

The contrast gap as can be seen from Figure 3 is larger for samples with larger atomic number Z.  This means that for samples with heavier atoms, the reduction of an amorphous layer on the entry side is even more critical in order to obtain a high-contrast ADF images using aberration-corrected probes.

The question that every person involved in sample preparation eventually asks is, “How much amorphous is too much?”  In an attempt to understand that question, the ADF image contrast was calculated for a set thickness of crystal Si with a varying layer of amorphous added to the exit surface of the crystal.  Figure 4 shows the resulting contrast values.

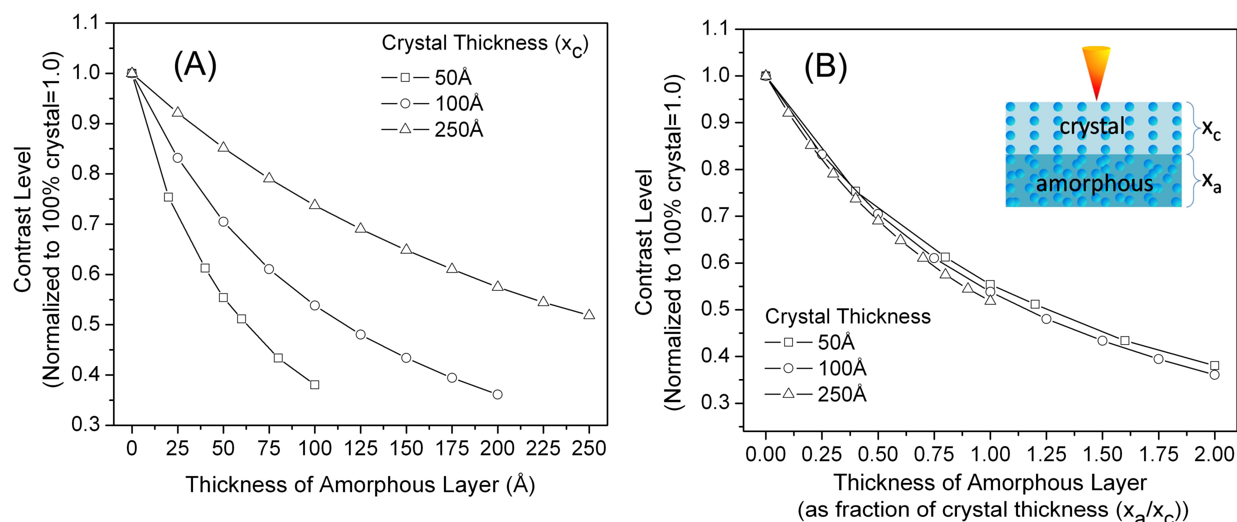


**Figure 4:** The ADF image contrast reduction in Si samples as a function of thickness is shown in two ways in these graphs. (A) shows the contrast level for three set thicknesses of crystal as an amorphous layer is placed on the exit surface and increased in thickness. (B) shows the same data plotted as a fraction of the amorphous thickness, $x_a$, to the crystal thickness, $x_c$. The inset in (B) demonstrates the arrangement of the sample with the beam.

Three thicknesses of crystal were used, but the behavior of the contrast reduction with the amorphous layer thickness is very similar for all three cases. Figure 4(A) shows the contrast level, normalized to the contrast value for pure crystal, as a function of the thickness of the amorphous layer. For 50 Å of crystal, the contrast is reduced to ~50% when 50 Å of amorphous is added. Similarly, the contrast for 100 Å is reduced by half when 100 Å of amorphous is added. This similarity is more marked when the contrast levels are plotted as a function of the fraction of the amorphous layer to the crystal layer, as shown in Figure 4(B). Now it is easier to see that all three lines follow the same basic trend. This shows that for any thickness of silicon crystal, the contrast reduction caused by an amorphous layer follows a simple trend that can be used to predict how much amorphous material is "too much". The values here cannot be transferred directly to experimental measurement, however, because these simulations do not take into account many additional contrast-reducing realities, including inelastic scattering, small sample tilts, and detector noise, among others.

## CONCLUSIONS

The contrast of ADF-STEM images are reduced to about half when a sample is 50% crystal and 50% amorphous, with only a slight further reduction in contrast when the amorphous layer is placed at the entry surface (and the probe is focused on the crystal layer at the center of the sample). The contrast reduction due to the orientation of the amorphous layer at the entry surface of the beam increases when the sample consists of atoms of higher Z-value. Further, the contrast reduction of an ADF-STEM image follows a simple trend as the amorphous layer increases, no matter what the thickness of the crystal layer.

## ACKNOWLEDGMENTS

This work is supported by the Nanoscale Science and Engineering Initiative of the NSF EEC-0117770 and NYSTAR C-020071. The authors would also like to thank Dr. E.J. Kirkland for providing various new mutislice codes used in these calculations.

## REFERENCES

[1] J.P. Benedict, R. Anderson, S.J. Klepeis and M. Chaker, Mat. Res. Soc. Symp. Proc. 199, 189 (1990).
[2] J.P. Benedict, R. Anderson, S.J. Klepeis, in: R. Anderson, B. Tracy, J. Bravman (Eds.), Specimen Preparation for Transmission Electron Microscopy of Materials II, Mat. Res. Soc. Vol. 254, Boston, MA, p. 121 (1992).
[3] S.J. Klepeis, J.P. Benedict and R.M. Anderson. In: J.C. Bravman, Editor, Specimen Preparation for Transmission Electron Microscopy of Materials, Mat. Res. Soc. Vol. 115, Pittsburgh, PA, p. 179 (1988).
[4] P.J. Goodhew, Thin Film Preparation for Electron Microscopy, in Practical Methods in Electron Microscopy, Vol. 11 (Elsevier, 1985).
[5] A. Barna, Mat. Res. Soc. Symp. Proc. 254, 3 (1992).
[6] K.A. Mkhoyan and J. Silcox, Appl. Phys. Lett. 82, 859 (2003).
[7] D.A. Muller and J. Silcox, Phil. Mag. A. 71, 1375 (1995).
[8] K.A. Mkhoyan, S.E. Maccagnano-Zacher, E.J. Kirkland, J. Silcox, Ultramicroscopy (submitted).
[9] J.M. Cowley, A.F. Moodie, Acta. Cryst. 10, 609 (1957).
[10] K.A. Mkhoyan, P.E. Batson, J. Cha, W.J. Schaff, J. Silcox, Science 312, 1354 (2006).